The diffusive ocean conveyor

Mark Holzer[1,2,3,4] and François W. Primeau[5]

Received 7 March 2006; revised 6 June 2006; accepted 9 June 2006; published 29 July 2006.

[1] We use a novel path-density transport diagnostic to trace out the deep branch of the ocean conveyor in a global circulation model. Our results suggest that the majority of the world's deep water is not transported back to the surface along the current systems of the standard great ocean conveyor (GOC). Standard GOC routes are evident only for waters with interior residence times, τ, less than about a thousand years, accounting for less than a quarter of the ventilation-to-re-exposure flux. Waters with longer τ are spread across the deep oceans by the "diffusive conveyor" and, by $\tau \sim 3000$ years, organized into a characteristic deep-North-Pacific pattern that is dominated by eddy diffusion. The observed depletion of oxygen and ^{14}C in the deep N Pacific is consistent with a diffusive conveyor and should not be interpreted as evidence of an advective terminus of the GOC deep branch. **Citation:** Holzer, M., and F. W. Primeau (2006), The diffusive ocean conveyor, *Geophys. Res. Lett.*, *33*, L14618, doi:10.1029/2006GL026232.

1. Introduction

[2] Broecker's great ocean conveyor (GOC) [*Broecker*, 1991] has become a paradigm for oceanic interbasin transport that is often used to interpret the global patterns of long-lived tracers. For example, the depletion of oxygen and ^{14}C in the deep N Pacific has been interpreted as locating the terminus of the GOC's deep branch [*Matsumoto and Key*, 2004; *England and Maier-Reimer*, 2001]. Similarly, the contrast in nutrient concentrations between the deep Atlantic and deep Pacific has been attributed to the continuous rain of organic matter accumulating in water parcels transported on the conveyor's lower limb [*Williams and Follows*, 2003]. The GOC schematic has become entrenched and is now standard in many textbooks [e.g., *Colling et al.*, 2004; *Bradley*, 1999; *Albaréde*, 2003].

[3] It is generally recognized, however, that Broecker's GOC is a rough schematic in need of refinement [*Schmitz*, 1995; *Toggweiler and Samuels*, 1993]. Indeed, a more complex picture of the global ocean circulation is beginning to emerge from a synthesis of recent hydrographic data [*Ganachaud and Wunsch*, 2000]. Recent work with coarse-resolution ocean models [*Drijfhout et al.*, 1996; *Speich et al.*, 2001; *Sun and Bleck*, 2001] has attempted to trace out the conveyor from the models' resolved velocities, while studies with time-averaged eddy-permitting models [e.g., *Drijfhout et al.*, 2003] explicitly calculate the effect of eddy correlations between velocity and isopycnal thickness. However, none of these studies accounts for the effectively diffusive transport of isopycnal turbulence.

[4] The notion common to most schematics of the interbasin circulation is that stately advection along the current systems of the deep oceans connects the North-Atlantic deep-water formation regions with the surface through upwelling and mixing in the Pacific and Southern Oceans. However, the extent to which this picture captures the global-scale surface-to-surface transport in the real ocean, or in ocean models, is unknown. Furthermore, the ocean also contains turbulent motion from the meso to the micro scale, whose effect is reasonably modelled by diffusion. The role of eddies in global-scale interbasin transport has never been quantified.

[5] We apply a novel transport diagnostic to trace advective-diffusive surface-to-surface paths in a global ocean model typical of those used in biogeochemical studies. Our diagnostic is the density of advective-diffusive paths connecting an entry/exit pair of surface patches. It is a joint density per unit volume and subsurface residence time, the time density being crucial as it reveals important information about transport rates. Applied to an entry patch in the N Atlantic (NA) and an exit patch in the Tropical Eastern Pacific (TEP), the diagnostic reveals the paths connecting the two basins partitioned according to residence time. We find that only the fast paths, accounting for less than half the flux of water connecting the NA formation region to the TEP surface, follow routes expected from the traditional GOC picture.

2. Path-Density and Its Conveyor Signature

[6] Our path-density diagnostic is ideally suited for revealing any conveyor signature of transport. First, consider fluid elements advected at constant speed v from point A to point B. The fluid may be thought of as being transported by a conveyor belt. The hallmark of such ideal conveyor transport is that, at any instant, each fluid element is characterized by the same residence time, regardless of its position on the conveyor. In particular, for every particle on the conveyor the time since last contact with A plus the time to first contact with B will give the same residence time $\tau = L/v$, where L is the conveyor length.

[7] For the general case where eddy motion imparts a random diffusive component to the particle motion, and different parts of the conveyor run at different speeds, one can characterize the conveyor by the local volume fraction $\eta(\mathbf{r}, \tau)\, d\tau$ of fluid elements that will eventually make it to B after a transit time, and hence residence time on the

[1]Department of Applied Physics and Applied Mathematics, Columbia University, New York, New York, USA.
[2]Also at NASA Goddard Institute for Space Studies, New York, New York, USA.
[3]Also at Department of Earth and Ocean Sciences, University of British Columbia, Vancouver, British Columbia, Canada.
[4]Also at Physics Department, Langara College, Vancouver, British Columbia, Canada.
[5]Department of Earth System Science, University of California, Irvine, California, USA.

0094-8276/06/2006GL026232$05.00

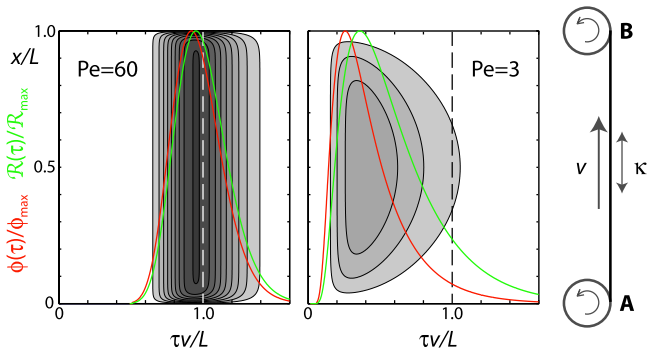

Figure 1. Shading: Contour plot of $\eta(x, \tau)$ for the idealized conveyor model of the schematic to the right. The contour interval is 0.25 v/L^2. The curves $\mathcal{R}(\tau)$ (green) and $\phi(\tau)$ (red) have been normalized by their peak values and superimposed.

conveyor, $\tau \in (\tau, \tau + d\tau)$. The more ideal the conveyor, the more sharply peaked η will be in τ and the less spatial variation η will have along the conveyor.

[8] We construct the path density η from the Green-function-based distributions $\mathcal{G}$ and $\widetilde{\mathcal{G}}$ of transit times since last, and to first contact, respectively, with specified surface patches. These distributions are computed as ideal tracers with imposed zero-concentration surface boundary conditions everywhere except over the entry patch for $\mathcal{G}$, or exit patch for $\widetilde{\mathcal{G}}$, where the boundary condition is a delta-function pulse in surface concentration [e.g., *Holzer and Hall*, 2000; *Primeau*, 2005]. Physically, $\mathcal{G}(\mathbf{r}, t_A|\Omega_A)dt_A$ is the probability that fluid elements at $\mathbf{r}$ had their last contact with surface patch Ω_A in the interval $(t_A, t_A + dt_A)$, and $\widetilde{\mathcal{G}}(\mathbf{r}, t_B|\Omega_B)dt_B$ is the probability that they will make their first surface contact at Ω_B in $(t_B, t_B + dt_B)$. Although our methodology applies to arbitrary time-dependent flows, we specialize to stationary flows here for simplicity.

[9] The probability $\eta d\tau d^3r$, that fluid in a volume element d^3r at $\mathbf{r}$ will make the A-to-B journey in a time interval $(\tau, \tau + d\tau)$, is essentially given by the product of $\mathcal{G}$ and $\widetilde{\mathcal{G}}$ summed over all times t_A and t_B that satisfy $t_A + t_B = \tau$. More precisely $\eta d\tau d^3r$ is given by $\mathcal{G}(\mathbf{r}, t_A|\Omega_A)\widetilde{\mathcal{G}}(\mathbf{r}, t_B|\Omega_B)$ $\delta(t_A + t_B - \tau)\, d\tau dt_A dt_B$ multiplied by the fractional volume element d^3r/V (the probability of finding fluid elements in d^3r, where V is the ocean volume), integrated over t_A and t_B. One obtains

$$\eta(\mathbf{r}, \tau, \Omega_A, \Omega_B) = \frac{1}{V}\int_0^\tau dt_A\, \mathcal{G}(\mathbf{r}, t_A|\Omega_A)\widetilde{\mathcal{G}}(\mathbf{r}, \tau - t_A|\Omega_B). \quad (1)$$

Each fluid element traces out a path as it travels from Ω_A to Ω_B, so that η is the joint path density, per unit volume and residence time, defined so that $\eta(\mathbf{r}, \tau, \Omega_A, \Omega_B)d\tau d^3r$ is the local volume fraction of fluid in d^3r at $\mathbf{r}$ that last ventilated on Ω_A, and will be re-exposed on Ω_B, after being in the ocean interior for a residence time $\tau \in (\tau, \tau + d\tau)$.

[10] For the interpretation of η it is helpful to consider the residence-time partitioned volume and flux of water that makes the Ω_A-to-Ω_B journey. Integrating η over the entire ocean volume, V, gives the residence-time partitioned transport-volume distribution, $\mathcal{R}$, that is, the fraction of V, per unit residence time, that was last ventilated on Ω_A and will be re-exposed on Ω_B:

$$\mathcal{R}(\tau, \Omega_A, \Omega_B) = \int_V d^3r \eta(\mathbf{r}, \tau, \Omega_A, \Omega_B). \quad (2)$$

The residence-time partitioned flux of Ω_A-to-Ω_B waters, per unit residence time, can then be obtained as [*Primeau and Holzer*, 2006]

$$\phi(\tau, \Omega_A, \Omega_B) = V\mathcal{R}(\tau, \Omega_A, \Omega_B)/\tau. \quad (3)$$

[11] It is instructive to consider a 1d model of advective-diffusive transport: A conveyor belt takes fluid at constant velocity v from $x = 0$ ("patch A") to $x = L$ ("patch B") in the presence of constant eddy diffusivity κ (Figure 1). The diffusion represents the continuum limit of fluid elements randomly walking back and forth on the conveyor. The behavior of η is governed by the Péclet number $\mathrm{Pe} \equiv Lv/\kappa$. In the purely advective limit, $\mathrm{Pe} \to \infty$, one recovers the expected ideal-conveyor result $\eta(x, \tau) = (1/L)\delta(\tau - L/v)$. For finite Pe, $\mathcal{G}$ and $\widetilde{\mathcal{G}}$ can be found using Laplace transforms, and the convolution (1) can be obtained as a series by expanding the product of transforms.

[12] Figure 1 shows $\eta(x,\tau)$ for the 1d model. For Pe = 60 advection dominates, η peaks near the advective time, v/L, and is nearly x-independent except for thin diffusive boundary layers. Nearly the entire available volume is ventilated on A and re-exposed on B, with $\int_0^\infty d\tau\mathcal{R}$ = 97%. For the large Pe = 60, diffusion broadens η symmetrically in τ. For Pe = 3, the effect of diffusion is more dramatic. The most probable A-to-B path is no longer via advection only, but B can be reached more quickly diffusively by particles with "eddy steps" that tend preferentially toward B. Hence, η is peaked at $\tau < v/L$. However, η is highly skewed toward long τ, because there are many more lengthy, random back-and-forth paths than short, mostly forward paths. For Pe = 3, $\int_0^\infty d\tau\mathcal{R}$ is reduced to 46% because some of the fluid ventilated on A is re-exposed again on A before reaching B and an equal amount of fluid is both ventilated and re-exposed on B. (The volume ventilated on B and re-exposed on A scales like $e^{-\mathrm{Pe}}$.) For finite Pe, the diffusive jitter of fluid elements reduces η to zero at the ends of the conveyor. For a given τ, the likelihood of not having been re-exposed must vanish as fluid gets close to either end.

3. Results From a Steady-State Ocean Model

[13] A steady-state off-line model was used to compute $\mathcal{G}$ and $\widetilde{\mathcal{G}}$ for the surface patches of the TransCom3 protocol as in the work by *Primeau* [2005]. The model is based on the time-averaged velocity and eddy-diffusivity tensor fields of a dynamical ocean general circulation model (OGCM) that uses the KPP [*Large et al.*, 1994] and GM [*Gent and McWilliams*, 1990] mixing schemes. The background dia- and isopycnal diffusivities are 0.5×10^{-5} and 1000 m^2/s. Second-order centered differences are used on a $\sim 3.75° \times 3.75°$ grid with 29 levels ranging in thickness from 50 m near the surface to 300 m near the bottom. The model has a velocity field and transport characteristics typical of similar

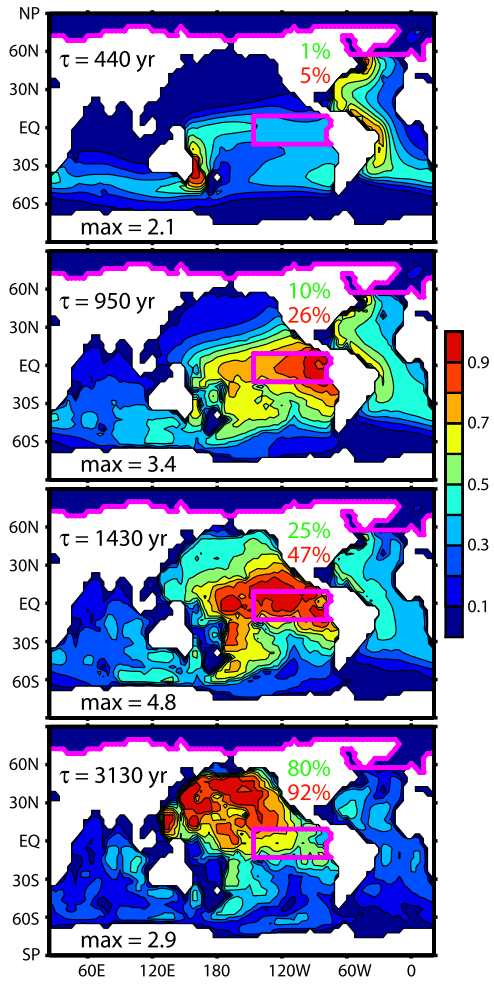

Figure 2. The depth-integrated path density for waters that had last surface contact on patch Ω_{NA}, and are destined to be re-exposed to the atmosphere on patch Ω_{TEP}. These patches are outlined in magenta. For each τ, the depth-integrated path density has been divided by its maximum value, max, indicated in units of 10^{-20} m^{-2} yr^{-1}. The top percentages (green) indicate the fractions of the total Ω_{NA}-to-Ω_{TEP} volume with residence times of τ or less. The bottom percentages (red) indicate the fractions of the total Ω_{NA}-to-Ω_{TEP} flux with residence times of τ or less.

resolution OGCM's and produces a maximum Atlantic meridional overturning stream function of 18 Sv (1 Sv $\equiv 10^6$ m^3/s).

[14] We focus on the deep-water paths that interconnect ocean basins. For brevity, we restrict attention to paths connecting the world oceans' dominant deep-water formation regions of the Southern Ocean (SO) and NA [*Ganachaud and Wunsch*, 2000] to the important upwelling sites of the SO and TEP [*Toggweiler and Samuels*, 1993; *Ganachaud and Wunsch*, 2000; *Primeau*, 2005; *Primeau and Holzer*, 2006], respectively. For our model, the total residence-time integrated fluxes from the NA patch, Ω_{NA}, to the surface of the Southern, Indian, and Pacific Oceans are 6.5, 1.1, and 1.2 Sv, respectively, with a flux from Ω_{NA} to the TEP patch, Ω_{TEP}, of 0.43 Sv. (See Figure 2 for definitions of Ω_{NA} and Ω_{TEP}.) The circuitous NA-to-TEP route captures most of the ocean's interbasin deep-water pathways, allowing us to illustrate the essential features of the diffusive conveyor with a minimum of surface-patch pairs.

[15] Figure 2 shows the depth-integrated density of paths connecting Ω_{NA} to Ω_{TEP} for four transit times ranging from relatively short to asymptotically long. (Although Ω_{NA} includes the entire Arctic Ocean, deepwater is only formed in the North-Atlantic part of Ω_{NA}.) Figure 2 may also be viewed as maps of the volume fraction of NA waters that make the journey to Ω_{TEP} in a time between τ and τ + 1 year. The overall picture is one where standard GOC routes dominate the interbasin transport only for short τ, accounting for less than about a quarter of the entire Ω_{NA}-to-Ω_{TEP} flux. For increasingly long residence times, the GOC routes become less and less apparent.

[16] For τ much less than ~1000 years, the path density is seen to trace out the current systems of the GOC deep branch (Figure 2 map for τ = 440 years): NA waters follow the deep western boundary current to the South Atlantic, where they join the circumpolar current, then branch off to follow the western boundary current along Australia and New Zealand toward the equator and shallower depths (~500 m, as seen in zonal averages, not shown). NA waters are then delivered to Ω_{TEP} by the Equatorial Undercurrent.

[17] The character of the path density, η, depends on where the residence time, τ, falls in the residence-time partitioned flux distribution, $\phi(\tau)$. For τ near the peak of $\phi(\tau)$, which occurs at τ_ϕ = 1180 years, the pattern of η becomes dominated by the position of Ω_{TEP}. This behavior is bracketed by the maps of Figure 2 for τ = 950 and 1430 years (corresponding to the 10% and 25% quantiles of $\mathcal{R}(\tau)$). The path density just beneath Ω_{TEP} must be highest at $\tau = \tau_\phi$ in order to produce the maximum re-exposure flux. (This behavior is also visible for the 1d model in Figure 1: At Pe = 3 the peak of $\phi(\tau)$ is at $\tau v/L$ = 0.26, for which the maximum near-boundary values of η occur.)

[18] For $\tau > \tau_\phi$, accounting for the remaining 64% of the total Ω_{NA}-to-Ω_{TEP} flux, any signature of the GOC becomes completely washed out (Figure 2 plots for τ = 1430 and 3130 years). Deep waters of NA origin with long τ are seen to populate the N Pacific. Zonal averages (not shown) reveal that as τ increases from 1000 to 3000 years, the regions of high path density move progressively deeper and further north. At $\tau \sim$ 3000 years, the bulk of the remaining ~20% of NA waters destined for the TEP lies below 2500 m in the N Pacific with a characteristic pattern that we call the deep-N-Pacific (DNP) pattern.

[19] Consistent with the emerging picture of the global circulation [*Toggweiler and Samuels*, 1993; *Ganachaud and Wunsch*, 2000; *Sun and Bleck*, 2001], a large fraction (28%) of our model ocean is both ventilated and re-exposed to the atmosphere on the SO surface, Ω_{SO}. The path-density diagnostic allows us to identify where SO waters venture before re-exposure on Ω_{SO}. Figure 3 shows the depth-integrated Ω_{SO}-to-Ω_{SO} path density at the 25, 50, and 90% quantiles of the associated transport-volume distribution. (We cannot quote meaningful quantiles of $\phi(\tau)$ because for overlapping entry and exit patches $\phi(\tau)$ has a non-integrable singular peak at τ = 0 [*Hall and Holzer*, 2003; *Primeau and Holzer*, 2006].) For τ less than a few hundred years, most of the water recirculates within the SO without straying far north. However, SO-to-SO waters with $\tau \sim$

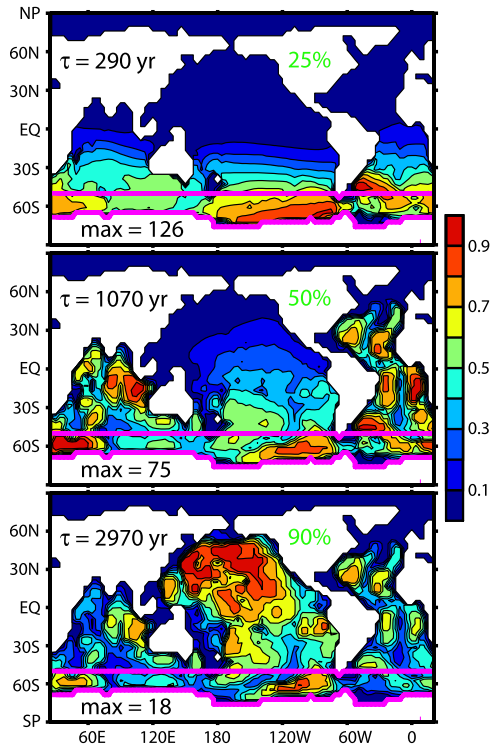

Figure 3. As Figure 2, but for waters that were both formed and re-exposed on Ω_{SO}, outlined in magenta. The percentages indicate the fractions of the total Ω_{SO}-to-Ω_{SO} volume with residence times of τ or less.

1000 years, are transported to the deep Indian and NA oceans. The N Pacific is penetrated by water of still longer residence times, and for $\tau \gtrsim 3000$ years, the remaining $\sim$10% of SO-to-SO waters are again organized into the DNP pattern.

[20] The emergence of the DNP pattern for $\tau \sim 3000$ years is found for all η connecting Ω_{NA} or Ω_{SO} with any exit patch, except those in the North and tropical Atlantic. In particular, the DNP pattern dominates the Ω_{NA}-to-anywhere, and the Ω_{SO}-to-anywhere path densities for $\tau \geq 3000$ years, which account for 11% and 14% of the corresponding transport volumes, respectively. Transport from Ω_{NA} or Ω_{SO} to the North and tropical Atlantic surface occurs primarily within the Atlantic with very little water straying into the other basins. The emergence of the DNP pattern is universal in the sense that it occurs for long-τ interbasin transport independent of the choice of patch pair. Physically, this reflects the fact that for long τ the eddy-diffusive "random walk" of fluid elements erases their memory of where they entered the interior and randomizes the eventual location of re-exposure to the atmosphere. As $\tau \to \infty$, one can show that η ultimately approaches the pattern of $\psi\tilde{\psi}$, where ψ and $\tilde{\psi}$ are the longest-lived modes of the transport operator and its adjoint. While $\psi\tilde{\psi}$ roughly resembles the DNP pattern, at $\tau = 3000$ years η has not yet converged to $\psi\tilde{\psi}$.

4. Conclusions

[21] Standard GOC routes are evident for residence times, τ, shorter than the residence time, τ_ϕ, of the peak of the flux-density distribution, and become washed out for $\tau > \tau_\phi$. Correspondingly, interbasin transport along the current systems of the GOC's deep branch accounts for only a minority of the total flux of NA deep waters to their TEP re-exposure location. The interbasin transport of waters with $\tau \sim 3000$ years is dominated by the "diffusive conveyor" which organizes the path density into the DNP pattern.

[22] Our new picture of a diffusive conveyor is expected to be qualitatively robust. While quantitative details will vary between models, one can expect to see a signature of the GOC's current systems for NA waters with $\tau < \tau_\phi$. Both circulation models [e.g., *Primeau and Holzer*, 2006] and tracer observations [e.g., *Waugh et al.*, 2004] point to the ocean being in a strong mixing regime with right-skewed transit-time distributions, and hence strongly right-skewed flux distributions $\phi(\tau)$. Eddy-resolving models will have faster and narrower boundary currents than coarse-resolution models, resulting in a potentially shorter τ_ϕ. However, to the extent that high-resolution models approximate the real ocean, resolved shear and turbulent dispersion of water is expected to impart long tails to the transit-time distributions, and hence to $\phi(\tau)$. Therefore, we expect waters with $\tau < \tau_\phi$ to account for only a minority of the interbasin surface-to-surface flux of deep waters in both ocean models and in the real ocean. The dominance of eddy diffusion in the deep N Pacific for long residence times is also expected to be robust, because long residence times occur for paths traversing the ocean's most stagnant regions that can only be accessed by eddies or slow localized dispersive currents whose effect is diffusive.

[23] Our results suggest that the observed depletion of oxygen and ^{14}C in the N Pacific results from eddy diffusion organizing long-residence-time waters into the DNP pattern, as opposed to indicating an advective terminus of the GOC's deep branch. This view is consistent with a global circulation in which deep currents either pass through the N Pacific without re-exposing their waters to the surface [*Toggweiler and Samuels*, 1993; *Schmitz*, 1995; *Ganachaud and Wunsch*, 2000], or possibly bypass the deep N Pacific entirely [*Sun and Bleck*, 2001]. Our analysis shows that eddy diffusion plays a crucial role in returning deep waters to the surface, and quantifies the extent to which the picture of the GOC captures the interbasin paths of deep water. While capturing the fast paths, standard GOC routes account for only a minor part of how the ocean communicates with the atmosphere and the rest of the climate system.

[24] **Acknowledgment.** We thank Tim Hall and Juno Hsu for comments. This work was supported by NSF grants ATM-04-32514 (MH) and OCE-0225156, ATM-0231380 (FP).

References

Albaréde, F. (2003), *Geochemistry: An Introduction*, 248 pp., Cambridge Univ. Press, New York.
Bradley, R. S. (1999), *Paleoclimatology: Reconstructing Climates of the Quaternary*, 613 pp., Elsevier, New York.
Broecker, W. S. (1991), The great conveyor belt, *Oceanography*, *4*, 79–89.
Colling, A., and Open University Course Team (2004), *Ocean Circulation*, 2nd ed., 286 pp., Elsevier, New York.
Drijfhout, S. S., E. Maier-Reimer, and U. Mikolajewicz (1996), Tracing the conveyor belt in the Hamburg large-scale geostrophic ocean general circulation model, *J. Geophys. Res.*, *101*, 22,563–22,575.
Drijfhout, S. S., P. de Vries, K. Döös, and A. C. Coward (2003), Impact of eddy-induced transport on the Lagrangian structure of the upper branch of the thermohaline circulation, *J. Phys. Oceanogr.*, *33*, 2141–2155.

England, M., and E. Maier-Reimer (2001), Using chemical tracers to assess ocean models, *Rev. Geophys.*, *39*, 29–70.

Ganachaud, A., and C. Wunsch (2000), Improved estimates of global ocean circulation, heat transport and mixing from hydrographic data, *Nature*, *408*, 453–457.

Gent, P. R., and J. C. McWilliams (1990), Isopycnal mixing in ocean circulation models, *J. Phys. Oceanogr.*, *20*, 150–155.

Hall, T. M., and M. Holzer (2003), Advective-diffusive mass flux and implications for stratosphere-troposphere exchange, *Geophys. Res. Lett.*, *30*(5), 1222, doi:10.1029/2002GL016419.

Holzer, M., and T. M. Hall (2000), Transit-time and tracer-age distributions in geophysical flows, *J. Atmos. Sci.*, *57*, 3539–3558.

Large, W. G., J. C. McWilliams, and S. C. Doney (1994), Oceanic vertical mixing: A review and a model with a nonlocal boundary layer parameterization, *Rev. Geophys.*, *32*, 363–403.

Matsumoto, K., and R. M. Key (2004), Natural radiocarbon distribution in the deep ocean, in *Global Environmental Change in the Ocean and on Land*, edited by M. Shiyomi et al., pp. 45–58, TERRAPUB, Tokyo.

Primeau, F. (2005), Characterizing transport between the surface mixed layer and the ocean interior with a forward and adjoint global ocean transport model, *J. Phys. Oceanogr.*, *35*, 545–564.

Primeau, F., and M. Holzer (2006), The ocean's memory of the atmosphere: Residence-time and ventilation-rate distributions of water masses, *J. Phys. Oceanogr.*, *36*, 1439–1456.

Schmitz, W. J. (1995), On the interbasin-scale thermohaline circulation, *Rev. Geophys.*, *33*, 151–173.

Speich, S., B. Blanke, and G. Madec (2001), Warm and cold water routes of an O.G.C.M. thermohaline conveyor belt, *Geophys. Res. Lett.*, *28*(2), 311–314.

Sun, S., and R. Bleck (2001), Thermohaline circulation studies with an isopycnic coordinate ocean model, *J. Phys. Oceanogr.*, *31*, 2761–2782.

Toggweiler, J. R., and B. Samuels (1993), New radiocarbon constraints on the upwelling of abyssal water to the ocean's surface, in *The Global Carbon Cycle*, *NATO ASI Ser. I, Global Environ. Change*, vol. 15, edited by M. Heinmann, pp. 333–366, Springer, New York.

Waugh, D. W., T. W. N. Haine, and T. M. Hall (2004), Transport times and anthropogenic carbon in the subpolar North Atlantic Ocean, *Deep Sea Res., Part I*, *51*, 1475–1491.

Williams, R. G., and M. J. Follows (2003), Physical transport of nutrients and the maintenance of biological production, in *Ocean Biogeochemistry*, edited by M. Fasham, pp. 19–51, Springer, New York.

M. Holzer, NASA Goddard Institute for Space Studies, 2880 Broadway, New York, NY 10025, USA. (mholzer@eos.ubc.ca)

F. W. Primeau, Department of Earth System Science, 3216 Croul Hall, University of California, Irvine, CA 92697-3100, USA. (fprimeau@uci.edu)